

UNIVERSIDAD SAN FRANCISCO DE QUITO USFQ

Colegio de Ciencias e Ingeniería

**Heat dissipated by a gold nano-shell
nanoparticle with a silica core**

Milena Sophia Mora Chaguay

Matemática

Trabajo de titulación presentado como requisito para la obtención del
título de Licenciado en Matemática

Quito, 14 de Diciembre de 2021

UNIVERSIDAD SAN FRANCISCO DE QUITO
USFQ

Colegio de Ciencias e Ingeniería

HOJA DE CALIFICACIÓN DE TRABAJO DE TITULACIÓN

Heat dissipated by a gold nano-shell nanoparticle with a silica core

Milena Sophia Mora Chaguay

Calificación:

Nombre del profesor, Título académico: Alessandro Veltri, Ph.D.

Firma del profesor

.....

Quito, 14 de Diciembre de 2021

Derechos de Autor

Por medio del presente documento certifico que he leído todas las Políticas y Manuales de la Universidad San Francisco de Quito USFQ, incluyendo la Política de Propiedad Intelectual USFQ, y estoy de acuerdo con su contenido, por lo que los derechos de propiedad intelectual del presente trabajo quedan sujetos a lo dispuesto en esas Políticas. Asimismo, autorizo a la USFQ para que realice la digitalización y publicación de este trabajo en el repositorio virtual, de conformidad a lo dispuesto en el Art. 144 de la Ley Orgánica de Educación Superior.

Firma del estudiante

Nombres y apellidos: Milena Sophia Mora Chaguay

Código: 00200882

Cédula de Identidad: 1724810609

Lugar y fecha: Quito, 14 Diciembre de 2021

ACLARACIÓN PARA PUBLICACIÓN

Nota: El presente trabajo, en su totalidad o cualquiera de sus partes, no debe ser considerado como una publicación, incluso a pesar de estar disponible sin restricciones a través de un repositorio institucional. Esta declaración se alinea con las prácticas y recomendaciones presentadas por el Committee on Publication Ethics COPE descritas por Barbour et al. (2017) Discussion document on best practice for issues around theses publishing, disponible en <http://bit.ly/COPETheses>.

UNPUBLISHED DOCUMENT

Note: The following capstone project is available through Universidad San Francisco de Quito USFQ institutional repository. Nonetheless, this project – in whole or in part – should not be considered a publication. This statement follows the recommendations presented by the Committee on Publication Ethics COPE described by Barbour et al. (2017) Discussion document on best practice for issues around theses publishing available on <http://bit.ly/COPETheses>.

“Aunque mi alma se suma en tinieblas, se alzaré en perfecta luz; he amado tanto las estrellas como para ser temeroso de la noche.”

–Sarah Williams, "El viejo astrónomo"

Dedicado a todas las niñas que, como yo, sueñan con ser científicas.

Agradecimientos

En primer lugar quiero agradecer a mi tutor Alessandro Veltri, quien con paciencia y dedicación me compartió sus conocimientos y me brindó su apoyo en cada una de las etapas de este proyecto. Gracias por ser mi puente entre la matemática y la física.

También quiero agradecer a la Universidad San Francisco de Quito, por acogerme como su estudiante y darme la oportunidad de aprender de tan increíbles profesores, en especial quienes conforman los departamentos de matemática y física. Este trabajo no hubiera sido posible sin todas sus enseñanzas. En particular quiero agradecer a Melissa Infusino, gracias por enseñarme a creer en las segundas oportunidades.

Adicionalmente, quiero agradecer a mis amigos Roberto Ávalos, Pablo Padilla y Adrián Vásquez, sin su ayuda este proyecto hubiera tardado más tiempo. A mis compañeros, en especial Ariana Soria, Alejandro Rueda. Y Mateo Martínez, gracias por motivarme y por ayudarme siempre que lo necesité.

Por último, quiero agradecer a mi familia, ustedes son mi pilar y mi fuerza para seguir adelante. A mi padre Fredy y a mi madre Sandra, gracias por siempre creer en mí y apoyarme en todas mis decisiones. A mis hermanas, María José y Romina, ustedes son mi motivación e inspiración. Y sobretodo a mi compañera incondicional, Alanis, quien estuvo a mi lado, no solo mientras realizaba este proyecto sino durante toda mi carrera.

Resumen

Teniendo en mente aplicaciones en termoplasmónica, en este trabajo estudiamos el calor disipado por una nanopartícula nano-shell, formada por un núcleo de sílica cubierto por un cascarón de oro. Utilizamos la aproximación cuasiestática para estudiar las densidades de campo eléctrico y de polarización del sistema. Además, aplicamos un tratamiento clásico para describir la interacción entre el metal y los campos. Consideramos el calor disipado del sistema desde un punto de vista electromagnético, tomando en cuenta la energía electrostática total en un medio lineal. Obtuvimos que el calor disipado adimensional por la nanopartícula está en el orden de 10^{16} , así como también que es necesario que el cascarón de oro sea fino para que su resonancia se encuentre en la parte infrarroja del espectro.

Palabras clave: Termoplasmónica, nanopartícula nano-shell, aproximación cuasiestática, calor disipado.

Abstract

Keeping in mind applications in thermoplasmonics, in this work we studied the heat dissipated by a nano-shell nanoparticle, which is formed by a gold shell coating a silica core. We used the quasistatic approximation to study the electric and polarization density fields of the system. Furthermore, we used a classical treatment to describe the interaction between the metal and the fields. We approached the heat dissipated by the system from an electromagnetic point of view, considering the total electrostatic energy in a linear medium. Obtained that the adimensional heat dissipated by the nanoparticle is in the order of 10^{16} , also that is necessary to use thin gold shell to obtain a resonance in the infrared part of the spectrum.

Keywords: Thermoplasmonics, nano-shell nanoparticle, quasistatic approximation, heat dissipated.

Contents

Lista de Figuras	11
1 Introduction	13
1.1 Plasmonics	13
1.1.1 Localized surface plasmon resonances	14
1.2 Thermoplasmonic Nanoparticles	15
1.2.1 Identifying the right thermoplasmonic nanoparticles	15
1.3 Plasmonic Photothermal Therapy	15
2 Preliminaries	17
2.1 Drude's Permittivity	17
2.1.1 Accounting for the losses due to interband transitions	20
3 Geometry of the Nanoparticle	22
3.1 The Electromagnetic Problem	22
3.2 Spherical Nanoparticle	24

	10
3.2.1 Using Math (and Physics) to unravel an ancient Magic . . .	31
3.3 Core-shell Nanoparticle	33
3.3.1 Nano-shells: tuning the resonance frequency	37
4 Heat	39
4.1 Back to the Electromagnetic Problem	40
4.2 Results	45
5 Conclusions	47
Bibliografia	47

List of Figures

1.1	Chartres Cathedral: stained-glass rose window	13
2.1	Drude's Model: the presence of an electric field drives the electrons in the opposite direction, the flux of electrons is slowed down because of the collision with the ions.	17
2.2	Complex permittivity for gold, calculated using a free electron model and including additional losses through the interpolation of the data measured by Johnson and Christy.	20
3.1	A material inclusion of permittivity ε_1 is dissolved in a host of permittivity ε_2	23
3.2	A spherical inclusion of permittivity ε_1 is dissolved in a host of permittivity ε_2	25
3.3	Lycurgus Cup is a 4th-century Roman glass cage cup	31
3.4	Nanoparticle found in the cup by TEM	32
3.5	Real and Imaginary parts of the Reduced Polarizability for a gold inclusion in glass.	32
3.6	A sphere of permittivity ε_1 in a shell of permittivity ε_2 , in a host of permittivity ε_3	33

3.7	Real and Imaginary parts of the Reduced Polarizability for a gold nanoshell with a silica core coated with a gold shell and dissolved in water. The polarizability is presented for different radius ratio: (a) $\rho = 0.35$; (b) $\rho = 0.5$; (c) $\rho = 0.75$;	37
4.1	(a) Adimensional Dissipated Heat for a gold nano-shell with a silica core and $\rho = 0.5$; (b) Real and imaginary part of the Reduced Polarizability for the same nanoparticle.	45
4.2	Adimensional Dissipated Heat Ω as a function of the radius ratio ρ and the energy for photon $\hbar\omega$	46

Chapter 1

Introduction

1.1 Plasmonics

Plasmonics is the study of the interactions between free electrons in metal and electromagnetic fields at the nanoscale [15]. While it has been used by humanity since centuries, as it was the physical phenomenon behind the colors of the stained glass windows of medieval cathedrals and the magic of roman artifacts, it is only after the full development of the classical electromagnetic theory that the mechanisms underlying Plasmonic phenomena were finally understood [3].

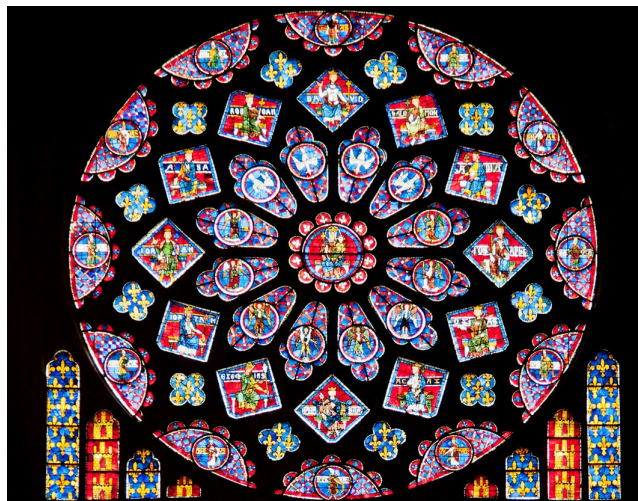


Figure 1.1: Chartres Cathedral: stained-glass rose window

After that, at the end of the last century, plasmonics emerged as an uprising field of research, but it was only in the last twenty years, with the development of a variety of new nano-technological methods [3], allowing to synthesize custom nanoparticles with nano scale precision that the interest of the scientific community on these phenomena begun growing at an exponential rate.

The main advantage of using metal nanoparticle to manipulate electromagnetic fields is their ability to confine an enormous light intensity in at a size much smaller than the wavelength when these nanoparticles while are being illuminated at their plasmonic resonance. This allows for an incredibly wide range of applications ranging from bio-sensing to photovoltaics, plasmon-enhanced spectroscopy and cancer-therapy [2]. Additionally, what makes interesting the electromagnetic confinement produced through plasmonics is that all of the information that can be encoded in the impinging light is transduced in this smaller-than-the-wavelength volume. This is obtained because when light incident on a metal can excite resonant coherent oscillations of the free electrons, thus information carried by a beam with a wavelength of some hundreds nanometers (e. g. information traveling in a optical fiber) can be stored and/or analyzed in a few nanometers.

In general, when discussing "plasmons", one can refer to three specific phenomena. 3D oscillation of the electron density which are referred as bulk plasmons; propagating surface plasmon polaritons (SPPs) which are oscillations that propagate across surfaces or along waveguides; and finally the electron oscillations that take place in illuminated metal nanoparticles which are called localized surface plasmon (LSPs) [11] and are the ones we will discuss in this Thesis .

1.1.1 Localized surface plasmon resonances

It exists a plethora of geometries that allows a metal nanoparticle to support a LSP, and all of them come with their strengths and flaws. As an example, spherical nanoparticles are more stable and allows for easier theoretical modelling, but they sports lower electromagnetic fields, while triangle or particles with spikes tends to produce more intense plasmonic fields, but can collapse easily when heated, etc. What is common in between all of the possible geometries is that, when the plasmon resonance is activated, a superficial electron density begins to oscillate through the skin of the particle creating a local electromagnetic field. Since metals have large electron densities, this field can be, in principle, very large. We will show in the following that this is a resonance phenomenon, so that in order to produce a plasmon the metal nanoparticle has to be excited at the right wavelength.

The frequency of the Localized Surface Plasmon Resonance (LSPR) can cover a range between the visible ultraviolet and near the infrared part of the spectrum. It depends of some geometrical parameters such as the shape and the size of the nanoparticle and it is influenced by the environment of the nanoparticle (i. e. the index of refraction of the solvent hosting the nanoparticles or, in the case of more convoluted structures on the index of refraction of dielectric inclusions).

If one wants to produce a LSPR in the visible range, the most viable plasmonic metals are silver and gold, which again comes with their advantages and disadvantages. Silver, as an example, shows low ohmic losses and thus is a better candidate for realizing plasmonic emitters [1], while gold nanoparticles are better suited for biological applications such as biolabels, because gold is biological compatible and its surface can be easily functionalized with different kind of molecules. Both metals are resistant to photo-damage and robust in terms of optical, chemical and thermal denaturation, however gold nanoparticles are stronger absorbers and therefore better suited for photothermal therapies [11].

1.2 Thermoplasmonic Nanoparticles

1.2.1 Identifying the right thermoplasmonic nanoparticles

It is not a trivial task to find the most suitable thermoplasmonic nanoparticle for a specific application, often is restricted to physical, chemical or biological constraints. For these reason we can adjust: the nanoparticle size, shape and composition. For example, we can maximize the light-to-heat conversion of the nanoparticles by increasing its size. Also, biological and biomedical applications require combining sizes of a few tens of nanometers in order to stimulate cellular uptake, with low toxicity and resonances in the NIR biological transparency window. Moreover, applications like catalysis and thermophotovoltaics emphasize high structural thermal stability [2].

1.3 Plasmonic Photothermal Therapy

Conventional cancer therapies such as surgery, chemotherapy or radiation, lack cancer cell specificity, meaning that they attack the overall cellular complex and harm the cancer cells more only because they tends to grow faster. While this is widely

recognized as a very effective approach, it also affect dramatically the growth of hair and fingernails. Moreover, some of them have actual deleterious side affects and are harmful and adversely impact the patient's overall well being [6].

In between the proposed alternatives to overcome these major problems, the use gold nanoparticles as photo-thermal agents stands out as one of one of the best candidate currently under consideration. The United States Food and Drug Administrations has, in fact, approved gold-based nanostructures as drug carriers or therapeutic agents for various phase-I clinical trials. Gold nanoparticles are of easy fabrication, have low cytotoxicity, offer tunable optical properties and can be surface modified in several ways. This last propriety allows them to be functionalized with antibodies, ligands, and other useful molecules that bind receptors on the membrane of cancer cells making them more easily absorbed from cancer cells, this is possible due to the presence of large gaps in the irregular vascular system of cancerous tissue, which are absent in health cells. This process leads to accumulation of gold particles in the tumor without affecting health tissue in the same area, this way allowing a targeting therapy. The accumulated gold nanoparticles are subsequently illuminated with a laser light with the wavelength within the tissue transparency window, in another words near the infrared spectrum. This light can usually penetrate 1-3[cm], which is sufficient for skin and breast cancers. Other cancer types can be addressed through endoscopy. The illumination and subsequent heating cause localized hyperthermia to the cancerous tissue, barely affecting the surrounding healthy tissue. Hyperthermia for cancer therapy has been successfully demonstrated in vivo in mouse, cat and dog. Moreover, it has been proceeded to clinical trials on human.

In this Thesis we will focus on nano-shell spherical particles, where an internal dielectric core is coated with a metal shell. The advantage of this geometry is that one can modulate the resonance frequency by varying the shell thickness (i. e. the ratio between the internal and the external radius) [5]. We will calculate the capacity of this structures of producing heat at different frequency, and we will show how throughout this characterization is possible, as an example, to identify the best radius ratio for Photothermal Therapy.

Chapter 2

Preliminaries

2.1 Drude's Permittivity

Before entering in the details of the geometry of the nanoparticle under study, let's discuss how the metal permittivity can be modeled by means of a free electron model describing the interaction between the electrons in the metal with the internal electric field.

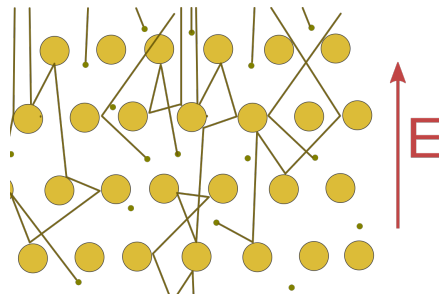


Figure 2.1: Drude's Model: the presence of an electric field drives the electrons in the opposite direction, the flux of electrons is slowed down because of the collision with the ions.

Let's consider a single electron of mass m_e and charge Q_e . When an optical field $\mathbf{E}(t)$ is acting on it, the electric force produced is given by:

$$\mathbf{F}_e(t) = Q_e \tilde{\mathbf{E}}(t). \quad (2.1)$$

because the electron moves in the metal, we will model the collision with the ions through a collision friction force (not different from the dragging friction force which act on a body moving through a viscous fluid). For this reason we define the friction coefficient η so that, using $\mathbf{v}(t)$ as the velocity of the electron. The collision friction force will be:

$$\mathbf{F}_r(t) = -2\eta\mathbf{v}(t). \quad (2.2)$$

If we now call to be the displacement of the electronic cloud within the metal with respect to the equilibrium position $\mathbf{r}(t)$, we can write the Newton's second law as:

$$m_e\mathbf{a}(t) = Q_e\tilde{\mathbf{E}}(t) - \eta\mathbf{v}(t) \quad (2.3)$$

which can be rearranged in the following second order differential equation:

$$\frac{d^2\mathbf{r}(t)}{dt^2} + 2\gamma\frac{d\mathbf{r}(t)}{dt} = \frac{Q_e}{m_e}\tilde{\mathbf{E}}(t) \quad (2.4)$$

$$\text{where } \gamma = \frac{\eta}{2m_e}.$$

If we now define the polarization produced in the metal as the sum of its passive and active part where the passive/dielectric part is due to the ions grid and the active to the electrons, we get:

$$\tilde{\mathbf{P}} = \varepsilon_0\chi_\infty\tilde{\mathbf{E}}(t) + \tilde{\mathbf{\Pi}}(t) \quad (2.5)$$

where $\mathbf{\Pi}(t) = n_eQ_e\mathbf{r}(t)$ and χ_∞ is the dielectric susceptibility of the ion's grid.

$$\frac{d^2\tilde{\mathbf{\Pi}}(t)}{dt^2} + 2\gamma\frac{d\tilde{\mathbf{\Pi}}(t)}{dt} = \frac{n_eQ_e^2}{m_e}\tilde{\mathbf{E}}(t) \quad (2.6)$$

Since, within the rotating wave approximation we have:

$$\tilde{\mathbf{E}}(t) = \frac{1}{2} [\mathbf{E}(t)e^{-i\omega t} + \mathbf{E}^*(t)e^{i\omega t}] \quad (2.7)$$

$$\tilde{\mathbf{\Pi}}(t) = \frac{1}{2} [\mathbf{\Pi}(t)e^{-i\omega t} + \mathbf{\Pi}^*(t)e^{i\omega t}], \quad (2.8)$$

here $\mathbf{E}(t)$ and $\mathbf{\Pi}(t)$ are, respectively the complex envelopes of the real electric field

$\tilde{\mathbf{E}}(t)$ and the real active polarization $\tilde{\mathbf{\Pi}}(t)$. We can conclude that

$$\frac{d\mathbf{\Pi}(t)}{dt} = \frac{d\mathbf{\Pi}(t)}{dt}e^{-i\omega t} - i\omega\mathbf{\Pi}(t)e^{-i\omega t} \quad (2.9)$$

$$\frac{d^2\mathbf{\Pi}(t)}{dt^2} = \frac{d^2\mathbf{\Pi}(t)}{dt^2}e^{-i\omega t} - 2i\omega\frac{d\mathbf{\Pi}(t)}{dt}e^{-i\omega t} - \omega^2\mathbf{\Pi}(t)e^{-i\omega t} \quad (2.10)$$

which yields

$$\frac{d^2\mathbf{\Pi}(t)}{dt^2} + 2(\gamma - i\omega)\frac{d\mathbf{\Pi}(t)}{dt} - (2i\gamma\omega + \omega^2)\mathbf{\Pi}(t) = \frac{n_e Q_e^2}{m_e}\mathbf{E}(t) \quad (2.11)$$

As the complex envelope $\mathbf{\Pi}(t)$ does not change very quickly, we can safely assume that $\frac{d^2\mathbf{\Pi}(t)}{dt^2} \approx 0$.

$$\frac{n_e Q_e^2}{m_e} \frac{\mathbf{E}(t)}{2(\gamma - i\omega)} = \frac{d\mathbf{\Pi}(t)}{dt} - \frac{\omega(2i\gamma + \omega)}{2(\gamma - i\omega)}\mathbf{\Pi}(t) \quad (2.12)$$

By (2.5), if we can find the steady state solution, then we can use the approximation $\frac{d\mathbf{\Pi}(t)}{dt} \approx 0$, which leads us to

$$\frac{n_e Q_e^2}{m_e} \frac{\mathbf{E}(t)}{2(\gamma - i\omega)} = -\frac{\omega(2i\gamma + \omega)}{2(\gamma - i\omega)}\mathbf{\Pi}(t) \quad (2.13)$$

Let the plasma frequency be defined as $\omega_{pl}^2 = \frac{n_e Q_e^2}{\varepsilon_0 m_e}$. Thus we got

$$\mathbf{\Pi}(t) = -\frac{\varepsilon_0 \omega_{pl}^2}{\omega(2i\gamma + \omega)}\mathbf{E}(t) \quad (2.14)$$

Replacing (2.14) in (2.5) we obtain that

$$\mathbf{P}(t) = \varepsilon_0 \left[\chi_\infty - \frac{\omega_{pl}^2}{\omega(2i\gamma + \omega)} \right] \mathbf{E}(t) \quad (2.15)$$

where the Drude's permittivity is

$$\varepsilon_m(\omega) = \varepsilon_\infty - \frac{\omega_{pl}^2}{\omega(2i\gamma + \omega)}. \quad (2.16)$$

2.1.1 Accounting for the losses due to interband transitions

The Drude permittivity calculated in the previous section, tends to underestimate the losses due to interband transitions. These are particularly important when evaluating the heat produced in a nanoparticle, for this reason, we will account for the additional losses calculating a $\varepsilon_\infty(\omega)$ as:

$$\varepsilon_\infty(\omega) = \varepsilon_m^{JC}(\omega) + \frac{\omega_{pl}^2}{\omega(\omega + 2i\gamma)} \quad (2.17)$$

where ε_m^{JC} is the dielectric permittivity of the metal calculated by interpolating the experimental data of Johnson and Christy [10], and using this one instead the static ε_∞ of the Drude model in formula 2.15.

The metal permittivity for gold, as calculated with formula 2.15 and including the additional losses, as discussed in this section, is presented in figure. 2.2 where the frequency dependence is measured in terms of the Energy per photon $\hbar\omega$ and presented in electronvolts.

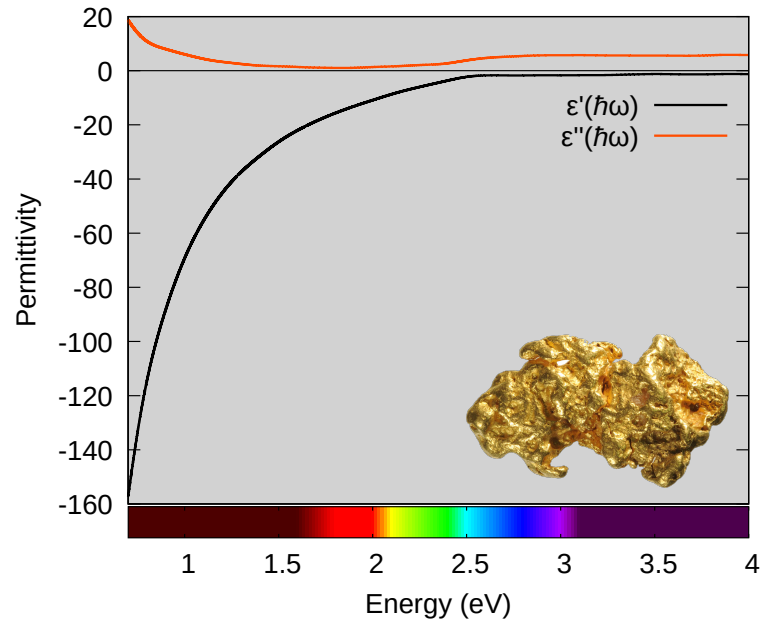


Figure 2.2: Complex permittivity for gold, calculated using a free electron model and including additional losses through the interpolation of the data measured by Johnson and Christy.

It is worth noting that, while the metal permittivity has required a suitable modeling to be discussed in a physically sound way; all the other materials that we will use in this characterization are dielectrics so, their electromagnetic response can be described as real constant numbers (e. g. water $\varepsilon_W = 1.7689$, silica $\varepsilon_S = 2.1316$, etc). Consequently, we can now focus on the effects due to the nanoparticle geometry which, due to the interface nature of the plasmons are as relevant as the material composing the nanostructure.

We will show in the following chapter that these shape effects can be modeled as the boundary conditions of a second order partial differential equation problem.

Chapter 3

Geometry of the Nanoparticle

3.1 The Electromagnetic Problem

The model in which we shall develop our theory is based on an optical approximation. Thus, we define the magnetic permeability as $\mu = \mu_0\mu_r$ (with $\mu_r \sim 1$). Although we are interested in time-dependent effects, we can omit the induction terms and the displacement current, as long as we consider the nanoparticle much smaller than the wavelength. This approximation called *the quasi static limit* is widely used when discussing small metal particles [19, 20, 5] and it is possible because, in this situation the exciting electric field can be considered uniform in the region of interest. In this approximation, the Maxwell's equations for reduces to:

$$\nabla \cdot \mathbf{E}(\mathbf{r}, t) = 0 \quad (3.1)$$

$$\nabla \times \mathbf{E}(\mathbf{r}, t) = 0 \quad (3.2)$$

which means there are no free charges, that is because of having two different mediums there is an electron migration in the opposite direction of the field. In other words, there is no net charge on the sphere, but there is polarization charge.

Knowing that $\nabla \times (\nabla f) = 0$, if $\nabla \times \mathbf{E} = 0$ it follows that $\mathbf{E} = \nabla f$.

Hence there exist $\Phi(\mathbf{r}, t)$ such that

$$\mathbf{E}(\mathbf{r}, t) = -\nabla\Phi(\mathbf{r}, t) \quad (3.3)$$

replacing in (3.1) we get

$$\nabla^2\Phi(\mathbf{r}, t) = 0 \quad (3.4)$$

where (3.4) is the Laplace equation.

This means that one can calculate the electric potential in any region of the considered space using Laplace equation and describe the presence of different materials by reconnecting Laplace equation's solution at the boundary in between the two materials. Specifically if, as in the example presented in figure 3.1 (i. e. a material inclusion in a solvent), one can solve equation 3.4 independently in the region of permittivity ε_1 and ε_2 and then evaluate the arbitrary coefficients of the general solution by imposing the boundary condition in between the two materials and at infinite.

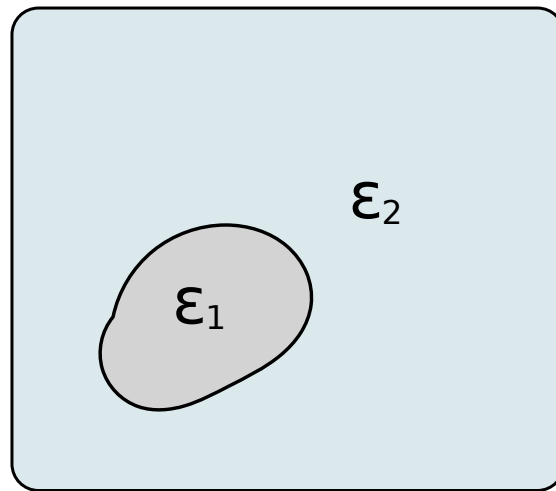


Figure 3.1: A material inclusion of permittivity ε_1 is dissolved in a host of permittivity ε_2 .

From a mathematical standpoint, the two-dimensional Laplace and its inhomogeneous version Poisson equations describe equilibrium configurations so they always appear in the context of boundary value problems. We seek a solution $u(x, y)$ defined at points belonging to a bounded, open domain, $\Omega \subset \mathbb{R}^2$. The solution is required to satisfy suitable conditions on the boundary of the domain, $\partial\Omega$, which will consist of one or more simple closed curves. The Dirichlet boundary conditions specify the value of the function u on the boundary $u(x, y) = h(x, y)$ for $(x, y) \in \partial\Omega$. Under mild regularity conditions on the domain Ω , the boundary values h , and the forcing function f , these conditions serve to uniquely specify the solution $u(x, y)$ to the Laplace or the Poisson equation. The Neumann boundary conditions $\frac{\partial u}{\partial \mathbf{n}} = \nabla u \cdot \mathbf{n} = k(x, y)$ on $\partial\Omega$ in which the normal derivative of the solution u is prescribed. In general, \mathbf{n} denotes the unit outwards normal to the boundary $\partial\Omega$, that

is the vector of unit length which is orthogonal to the tangent to the boundary and points away from the domain. [17].

Returning to our problem, we can divide space in a internal volume 1 (the one where the material inclusion is) and an external volume 2 (the complementary space), in both cases we have to solve a second order differential equation which has a well defined solution in a closed space if boundary conditions of Neumann or Dirichlet are known on the enclosing surface [17]. It is important to mention here that, while region 1 is evidently a section of space enclosed by a surface, in the case of region 2 this is not as much evident. The way to face this apparent incongruity is to deal with the exciting field as a boundary condition set on a spherical surface of infinite radius. Being the electric field related to the gradient of the potential this corresponds to a Neumann condition on the external boundary which is enough to overcome the empanse.

3.2 Spherical Nanoparticle

“Everything is a sphere, if you’re brave enough approximating”

— Anonymous Physicist

The more complex the shape of the surface identifying the boundary between the inclusion and the solvent, the more advanced has to be the mathematical tool to allow its description. While advanced methods such as the T-Matrix [14] exists to manage nanoparticles with extremely exotic shapes (up to complex agglomerate of different particles); we will focus our study on the simplest configuration of the spherical particle. This not only represent a first approximation of a vast variety of shapes, it also constitute a class of very stable nanoparticles suitable for thermal applications (that will be the focus of the last part of this Thesis) because, when heated over a threshold, most of the metal nanoparticles tends collapse into spheres.

Let’s consider a spherical nanoparticle of radius a with electric permittivity ε_1 embedded in a solvent with electric permittivity ε_2 . The whole system is excited through a local uniform electric field \mathbf{E}_0 . For the sake of simplicity we position the center of the spherical nanoparticle in the origin of the system of reference and the exciting field alongside the z -axis, so that the surface S identifying the boundary in

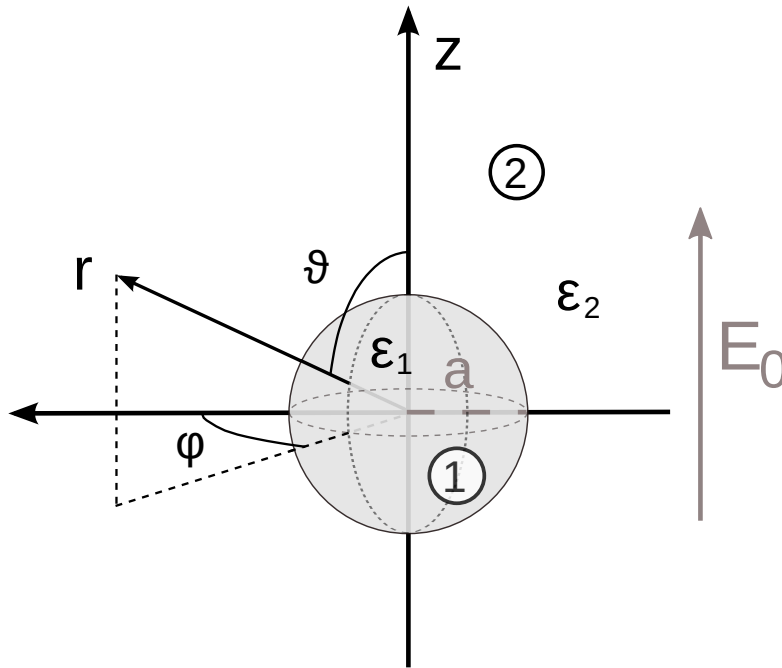


Figure 3.2: A spherical inclusion of permittivity ε_1 is dissolved in a host of permittivity ε_2 .

between the two media given by the equation:

$$r = a, \quad (3.5)$$

where $r = \sqrt{x^2 + y^2 + z^2}$ is the radial spherical coordinate, while the exciting field is given by

$$\mathbf{E}_0 = E_0 \hat{\mathbf{k}}, \quad (3.6)$$

Now our problem turns into solving the Laplace equation inside (region 1) and outside the sphere (region 2). As mentioned in the previous section, the reconnection with the excitation field can be treated as a given boundary condition on a spherical surface of infinite radius. Considering that the relation between the electric field and the electric potential is given by:

$$\mathbf{E}(\mathbf{r}) = -\nabla\Phi(\mathbf{r}), \quad (3.7)$$

it is trivial to show that the electric field presented in equation 3.6 correspond to the potential:

$$\Phi_0 = -E_0 z, \quad (3.8)$$

in spherical coordinate:

$$\Phi_0 = -E_0 r \cos \theta. \quad (3.9)$$

Using the Laplace operator in spherical coordinates, which is given by

$$\nabla^2 = \frac{1}{r^2 \sin(\theta)} \left[\sin(\theta) \frac{\partial}{\partial r} \left(r^2 \frac{\partial}{\partial r} \right) + \frac{\partial}{\partial \theta} \left(\sin(\theta) \frac{\partial}{\partial \theta} \right) + \frac{1}{\sin(\theta)} \frac{\partial^2}{\partial \varphi^2} \right] \quad (3.10)$$

in equation 3.4 and noting that the system has azimuthal symmetry and that time dependence can be treated in the rotating wave approximation, then

$$\Phi(r, \theta, \varphi, t) = \Phi(r, \theta) e^{-i\omega t}, \quad (3.11)$$

Which leads us to the following equation:

$$\frac{\partial}{\partial r} \left[r^2 \frac{\partial}{\partial r} \Phi(r, \theta) \right] + \frac{1}{\sin(\theta)} \frac{\partial}{\partial \theta} \left[\sin(\theta) \frac{\partial}{\partial \theta} \Phi(r, \theta) \right] = 0. \quad (3.12)$$

This last equation has to be solved independently for Φ_1 and Φ_2 . However, both will be solution of the same homogeneous differential equation, so we can build the same base of solution and then specify the differences in between them by adjusting the coefficients of the linear combination by means of the boundary conditions.

Equation 3.12 can be solved by separation of variables since its boundary conditions are homogeneous [17].

$$\Phi(r, \theta) = R(r)\Theta(\theta) \quad (3.13)$$

Replacing (3.13) in (3.12) we get

$$\Theta(\theta) \frac{\partial}{\partial r} \left(r^2 \frac{\partial}{\partial r} [R(r)] \right) + R(r) \frac{1}{\sin(\theta)} \frac{\partial}{\partial \theta} \left(\sin(\theta) \frac{\partial}{\partial \theta} [\Theta(\theta)] \right) = 0 \quad (3.14)$$

Dividing by (3.12)

$$\frac{1}{R(r)} \frac{\partial}{\partial r} \left(r^2 \frac{\partial}{\partial r} [R(r)] \right) + \frac{1}{\Theta(\theta)} \frac{1}{\sin(\theta)} \frac{\partial}{\partial \theta} \left(\sin(\theta) \frac{\partial}{\partial \theta} [\Theta(\theta)] \right) = 0 \quad (3.15)$$

Defining

$$\ell(\ell + 1) = \frac{1}{R(r)} \frac{\partial}{\partial r} \left(r^2 \frac{\partial}{\partial r} [R(r)] \right) \quad (3.16)$$

$$-\ell(\ell + 1) = \frac{1}{\Theta(\theta)} \frac{1}{\sin(\theta)} \frac{\partial}{\partial \theta} \left(\sin(\theta) \frac{\partial}{\partial \theta} [\Theta(\theta)] \right) \quad (3.17)$$

We can rewrite (3.16) to obtain

$$R''(r) + \frac{2}{r} R'(r) - \frac{1}{r^2} \ell(\ell + 1) R(r) = 0 \quad (3.18)$$

We can solve this using Frobenius's method. Taking $y(x) = \sum_{j=0}^{\infty} a_j x^{s+j}$ and replacing it on (3.18) we get

$$\sum_{j=0}^{\infty} a_j r^{s+j-2} [(s+j)(s+j+1) - \ell(\ell+1)] = 0 \quad (3.19)$$

Therefore for $j = 0$ and r^{s-2} we get the following indicial equation

$$a_0 [s(s+1) - \ell(\ell+1)] = 0 \quad (3.20)$$

And knowing that $a \neq 0$ we obtain as solutions $s = -(\ell + 1)$ and $s = \ell$. Therefore our general solution for the coordinate r is

$$R(r) = Ar^\ell + B \frac{1}{r^{\ell+1}} \quad (3.21)$$

Back to the second equation (3.17) doing the change of variable $u = \cos(\theta)$, we got the following Legendre equation

$$(1 - u^2) \frac{d^2 P(u)}{du^2} - 2u \frac{dP(u)}{du} + P(u) \ell(\ell + 1) = 0 \quad (3.22)$$

whose solution is $P(u) = P_\ell(u)$. Reapplying the change of variable we obtain the general solution for the coordinate θ

$$\Theta(\theta) = P_\ell(\cos(\theta)) \quad (3.23)$$

Multiplying the solutions for the coordinates r and θ and expressing it as a linear combination we get the general solution for the electric potential

$$\Phi(r, \theta) = \sum_{\ell=0}^{\infty} \left(A_{\ell} r^{\ell} + B_{\ell} \frac{1}{r^{\ell+1}} \right) P_{\ell}(\cos(\theta)) \quad (3.24)$$

We can now use the boundary conditions to determine the coefficients A_{ℓ} and B_{ℓ} specifying the two solution inside and outside the metal nanoparticle.

It can be worth mentioning that, since we are working with two spherical surfaces: the internal one, on which the value of the electric potential is known, and its derivative (i. e. the radial component of the electric field) is discontinuous, which can be identified as a Dirichlet and the external one where it was the field that was known and that consequently can be identified as a Neumann one.

In region 1, since we have $r = 0$, to avoid divergence we have to set $B_{1\ell} = 0$.

$$\Phi_1(r, \theta) = \sum_{\ell=0}^{\infty} A_{1\ell} r^{\ell} P_{\ell}(\cos(\theta)) \quad (3.25)$$

As discussed at the beginning of this section, in region 2, since we have to satisfy

$$\lim_{r \rightarrow \infty} \Phi_2(r, \theta) = -E_0 r \cos(\theta), \quad (3.26)$$

for doing this, we set $A_{2\ell} = 0 \forall \ell \neq 1$. Knowing that $P_{\ell}(\cos(\theta)) = \cos(\theta)$ therefore

$$\Phi_2(r, \theta) = \sum_{\ell=0}^{\infty} B_{2\ell} \frac{1}{r^{\ell+1}} P_{\ell}(\cos(\theta)) - E_0 r \cos(\theta). \quad (3.27)$$

Considering the boundary condition for $r = a$, which means that

$$\Phi_1(a, \theta) = \Phi_2(a, \theta); \quad (3.28)$$

applying the uniqueness of power series we got that:

$$A_{1\ell} = \frac{B_{2\ell}}{a^{2\ell+1}} - \delta_{\ell 1} E_0, \quad (3.29)$$

then

$$\Phi_1(r, \theta) = \sum_{\ell=0}^{\infty} \left[\frac{B_{2\ell}}{a^{2\ell+1}} - \delta_{\ell 1} E_0 \right] r^\ell P_\ell(\cos(\theta)) \quad (3.30)$$

and

$$\Phi_2(r, \theta) = \sum_{\ell=0}^{\infty} \frac{B_{2\ell}}{r^{\ell+1}} P_\ell(\cos(\theta)) - E_0 r \cos(\theta). \quad (3.31)$$

Now considering the boundary condition about the radial continuity, which means that

$$\varepsilon_1 E_{1r} \Big|_{r=a} = \varepsilon_2 E_{2r} \Big|_{r=a}; \quad (3.32)$$

using the fact that

$$E_{1r} = -\frac{\partial \Phi_1}{\partial r} = -\sum_{\ell=0}^{\infty} \ell \left[\frac{B_{2\ell}}{a^{2\ell+1}} - \delta_{\ell 1} E_0 \right] r^{\ell-1} P_\ell(\cos(\theta)), \quad (3.33)$$

and

$$E_{2r} = -\frac{\partial \Phi_2}{\partial r} = \sum_{\ell=0}^{\infty} (\ell + 1) \frac{B_{2\ell}}{r^{\ell+2}} P_\ell(\cos(\theta)) + E_0 \cos(\theta), \quad (3.34)$$

and, applying the uniqueness of power series we got that:

$$B_{2\ell} = a^{\ell+2} \frac{\ell \varepsilon_1 a^{\ell-1} - \varepsilon_2}{\varepsilon_1 \ell + (\ell + 1) \varepsilon_2} E_0 \delta_{\ell 1}. \quad (3.35)$$

Notice that the Kronecker delta $\delta_{\ell 1}$ is equal to 0 when $\ell \neq 1$, meaning that this configuration will only activate the term with $\ell = 1$ (i. e. the dipolar one). Moreover, by taking this into account in equation 3.35 we get:

$$B_{21} = a^3 \frac{\varepsilon_1 - \varepsilon_2}{\varepsilon_1 + 2\varepsilon_2}; \quad (3.36)$$

Which finally leads to the solutions:

$$\Phi_1(r, \theta) = -\frac{3\varepsilon_2}{\varepsilon_1 + 2\varepsilon_2} E_0 r \cos(\theta) \quad (3.37)$$

and

$$\Phi_2(r, \theta) = \left[\frac{a^3}{r^3} \frac{\varepsilon_1 \varepsilon_2}{\varepsilon_1 + 2\varepsilon_2} - 1 \right] E_0 r \cos(\theta). \quad (3.38)$$

We will now use this result to find the polarizability α . This physical quantity is related to all the optical properties of the nanoparticle and it is defined as the complex constant of proportionality in between the dipole moment of the nanoparticle and the exciting field:

$$\mathbf{p} = \alpha(\omega)\mathbf{E}_0. \quad (3.39)$$

In order to recover $\alpha(\omega)$ we only focus on the potential for the region 2, which is the one where the nanoparticle dipolar field is.

Recalling that the dipole moment of the nanoparticle is related to its electric potential, through the formula:

$$\Phi_{dip}(r, \theta) = \frac{\hat{r} \cdot \mathbf{p}}{4\pi\epsilon r^2} = \frac{p \cos(\theta)}{4\pi\epsilon r^2}, \quad (3.40)$$

and noticing that for the potential Φ_2 there are two terms: One (the first) corresponding to the field that affects the nanoparticle and another (the second) corresponding to the dipolar field produced around the nanoparticle, one can identify:

$$\frac{B_{21} \cos(\theta)}{r^2} = \frac{p \cos(\theta)}{4\pi\epsilon_2 r^2}, \quad (3.41)$$

which corresponds to the dipolar potential as presented in equation 3.40, when, as in the described case the dipole is oriented along the z -axis

$$\mathbf{p} = p\hat{\mathbf{k}}. \quad (3.42)$$

Therefore, solving equation 3.41 for p , and knowing that $\alpha = \frac{p}{E}$ we obtain:

$$\alpha = \frac{B_{21}(4\pi\epsilon_2)}{E_0} \quad (3.43)$$

Finally, replacing the value obtained for the coefficient B_{21} in equation 3.36 we finally get an expression for the nanoparticle polarizability:

$$\alpha(\omega) = 4\pi\epsilon_2 a^3 \frac{\epsilon_1(\omega) - \epsilon_2}{\epsilon_1(\omega) + 2\epsilon_2}. \quad (3.44)$$

It is very important to mention here, that because metals can show a negative real part of their permittivity (see figure 2.2 in the previous chapter), one can choose an

appropriate dielectric so that a resonant ω_R exist such that:

$$\text{Re}[\varepsilon_1(\omega_R)] + 2\varepsilon_2 = 0 \quad (3.45)$$

which produces a resonant peak at ω_R . It might worth mentioning that this will not be a singularity because of the imaginary part of $\varepsilon_1(\omega)$, which as one can see in equation 2.16 is related to γ and thus to the losses due to the collisions with the ions.

It is also possible, by looking at figure 2.2 and comparing the range of $\varepsilon_1(\omega)$ provided by gold inclusions, that common dielectrics such as water ($\varepsilon_2 = 1.7689$), silica ($\varepsilon_2 = 2.1316$) and glass ($\varepsilon_2 = 1.2247$) can provide localized plasmonic resonances in the visible range.

3.2.1 Using Math (and Physics) to unravel an ancient Magic

The oldest known instance making use of Localized Surface Plasmons Resonances is a roman artifact dating from the 4th-century : the Lycurgus Cup (fig. 3.3). It is a Cup surrounded by a frieze showing the myth of Lycurgus, a king who defied god Dionysus by killing his follower Ambrosia. Dionysus avenges Ambrosia by turning her corpse in a vine who tears apart the body of the scornful king. When the cup



Figure 3.3: Lycurgus Cup is a 4th-century Roman glass cage cup

is illuminated from the outside, it shows a deep green color recalling the vines Ambrosia's body was turned into. However, if a candle is lowered into it, it turns in a shining red, echoing the blood of King Lycurgus.

It has been suggested that, this not very common scene, was meant to evoke the ripening of red grapes, which can be easily related with Dionysus being the god of Wine.

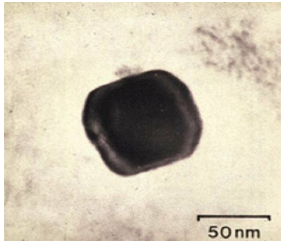


Figure 3.4: Nanoparticle found in the cup by TEM

The cup itself is made of glass, but Analytical Transmission electron Microscopy revealed the presence of minute particles of metal, typically 50 – 100 nm in diameter. X-ray analysis showed that these nanoparticles were silver-gold alloy (see figure 3.4). Approximating the metal inclusions with spherical nanoparticles and assuming that the silver component in the alloy is negligible, we can use the results developed in the previous section to explain the mysteries of this ancient cup.

We will use the metal permittivity as calculated in equation 2.16, taking into account the additional losses due to interband transitions as described in equation 2.17 to evaluate the permittivity $\varepsilon_1(\omega)$ in equation 3.44, while we will use $\varepsilon_2 = 1.2247$ to account that the matrix in which, this inclusions are embedded is made of glass. The result of this calculation is presented in figure 3.5 as a plot of the real and the imaginary part of the reduced polarizability $\frac{\alpha}{4\pi\varepsilon_2 a^3}$.

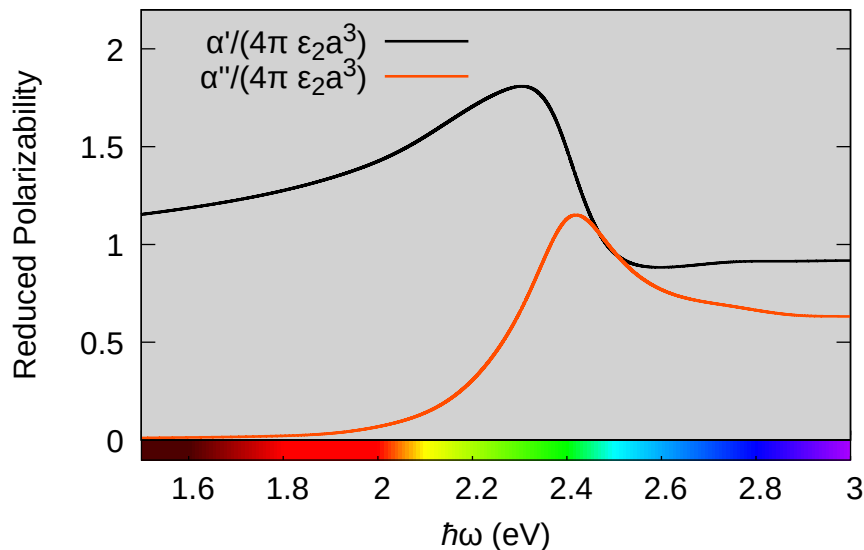


Figure 3.5: Real and Imaginary parts of the Reduced Polarizability for a gold inclusion in glass.

Here one can appreciate that the Localized Plasmon Resonance occurs around $\hbar\omega \sim 2.4$ eV corresponding to the green section of the visible spectrum.

As mentioned before, the polarizability is related to all of the relevant optical properties of an inclusion and it is possible to show [4] that the absorption and the scattering cross-section of a nanoparticle are respectively:

$$\sigma_a = 2\pi \frac{\alpha''}{\lambda \epsilon_2}, \quad (3.46)$$

$$\sigma_s = \left(\frac{2\pi}{\lambda}\right)^2 \frac{|\alpha|^2}{6\pi \epsilon_2^2}. \quad (3.47)$$

the absorption cross-section σ_a is proportional to the imaginary part of the polarizability α'' , while the scattering cross section σ_s is proportional to the norm of the polarizability $|\alpha|^2$. Both are thus their maximum at the LSPR, meaning that a medium realized in glass including gold impurities will absorb and scatter the green part of the spectrum.

Therefore, when the cup is illuminated from the outside, the scattered green light will make it look green, while, when a light source is put inside of it, all the green section of the spectrum will be absorbed letting pass only is complementary color which is red.

3.3 Core-shell Nanoparticle

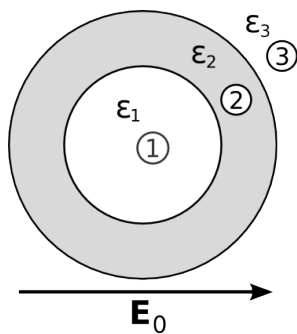


Figure 3.6: A sphere of permittivity ϵ_1 in a shell of permittivity ϵ_2 , in a host \mathfrak{B} of permittivity ϵ_3

We will now extend our problem to an spherical core-shell nanoparticle formed by a central core with permittivity ϵ_1 and radius a_1 and a shell with permittivity ϵ_2 and external radius a_2 (see fig 3.6). The outside of the core-shell has an electric permittivity ϵ_3 .

As before we will consider to be in the *quasi static limit* so the core-shell sphere is excited by a uniform electric field. We will again put the origin of our system of coordinated in the center of the spheres

and consider the exciting fields along the z -axis

$$\mathbf{E}_0 = E_0 \hat{\mathbf{k}}$$

As in the nanoparticle problem we are in optical approximation, we have a system with azimuthal symmetry and the time dependence is discussed separately. Solving the Laplace equation in spherical coordinates in any of the three considered regions, we got the general solution for the electric potential demonstrated in section 3.2:

$$\Phi(r, \theta) = \sum_{\ell=0}^{\infty} \left(A_{\ell} r^{\ell} + B_{\ell} \frac{1}{r^{\ell+1}} \right) P_{\ell}(\cos(\theta)). \quad (3.48)$$

To obtain the coefficients we will, once again make use the boundary conditions. As with the nanoparticle system we have Dirichlet boundary conditions, since we are working with a core-shell sphere in a constant electric field we have to specify the solutions for the potential in three regions:

In region 1, since we have $r = 0$, to avoid divergence let $B_{1\ell} = 0$:

$$\Phi_1(r, \theta) = \sum_{\ell=0}^{\infty} A_{1\ell} r^{\ell} P_{\ell}(\cos(\theta)). \quad (3.49)$$

In region 2, we haven't any specifics yet, because the solution in this region needs to reconnect to the other two: In region 3, since we have to satisfy

$$\lim_{r \rightarrow \infty} \Phi_3(r, \theta) = -E_0 r \cos(\theta) \quad (3.50)$$

we will set $A_{3\ell} = 0 \forall \ell \neq 1$. Knowing that $P_{\ell}(\cos(\theta)) = \cos(\theta)$ therefore

$$\Phi_3(r, \theta) = \sum_{\ell=0}^{\infty} B_{3\ell} \frac{1}{r^{\ell+1}} P_{\ell}(\cos(\theta)) - E_0 r \cos(\theta). \quad (3.51)$$

We will now take into account the continuity on the two interfaces at $r = a_1$ and $r = a_2$. The boundary condition for $r = a_1$ means that:

$$\Phi_1(a_1, \theta) = \Phi_2(a_1, \theta), \quad (3.52)$$

Applying the uniqueness of power series we got that:

$$A_{1\ell} = \frac{B_{2\ell}}{a_1^{2\ell+1}} + A_{2\ell}, \quad (3.53)$$

thus

$$\Phi_1(r, \theta) = \sum_{\ell=0}^{\infty} \left[\frac{B_{2\ell}}{a_1^{2\ell+1}} + A_{2\ell} \right] r^\ell P_\ell(\cos(\theta)) \quad (3.54)$$

and

$$\Phi_2(r, \theta) = \sum_{\ell=0}^{\infty} \left(A_{2\ell} r^\ell + B_{2\ell} \frac{1}{r^{\ell+1}} \right) P_\ell(\cos(\theta)). \quad (3.55)$$

When considering the boundary condition at $r = a_2$, we have:

$$\Phi_2(a_2, \theta) = \Phi_3(a_2, \theta), \quad (3.56)$$

again, applying the uniqueness of power series we get:

$$A_{2\ell} = \frac{B_{3\ell} - B_{2\ell}}{a_2^{2\ell+1}} - E_0 \delta_{1\ell}, \quad (3.57)$$

thus

$$\Phi_2(r, \theta) = \sum_{\ell=0}^{\infty} \left(A_{2\ell} r^\ell + \left[\frac{B_{3\ell} - B_{2\ell}}{a_2^{2\ell+1}} - E_0 \delta_{1\ell} \right] \frac{1}{r^{\ell+1}} \right) P_\ell(\cos(\theta)) \quad (3.58)$$

and

$$\Phi_3(r, \theta) = \sum_{\ell=0}^{\infty} B_{3\ell} \frac{1}{r^{\ell+1}} P_\ell(\cos(\theta)) - E_0 r \cos(\theta) \quad (3.59)$$

We have now to impose the radial continuity, which means that

$$\varepsilon_1 E_{1r} \Big|_{r=a_1} = \varepsilon_2 E_{2r} \Big|_{r=a_1}, \quad (3.60)$$

$$\varepsilon_2 E_{2r} \Big|_{r=a_2} = \varepsilon_3 E_{3r} \Big|_{r=a_2}; \quad (3.61)$$

therefore using the fact that $E_r = -\frac{\partial\Phi}{\partial r}$ we get:

$$E_{1r} = -\sum_{\ell=0}^{\infty} \ell \left[\frac{B_{2\ell}}{a_1^{2\ell+1}} + A_{2\ell} \right] r^{\ell-1} P_{\ell}(\cos(\theta)) \quad (3.62)$$

$$E_{2r} = -\sum_{\ell=0}^{\infty} \left(\ell A_{2\ell} r^{\ell-1} + (\ell+1) \left[\frac{B_{3\ell} - B_{2\ell}}{a_2^{2\ell+1}} - E_0 \delta_{1\ell} \right] \frac{1}{r^{\ell+2}} \right) P_{\ell}(\cos(\theta)) \quad (3.63)$$

$$E_{3r} = -\sum_{\ell=0}^{\infty} (\ell+1) \frac{B_{3\ell}}{r^{\ell+2}} P_{\ell}(\cos(\theta)) + E_0 \cos(\theta) \quad (3.64)$$

Once again, applying the uniqueness of power series, and defining the radius ratio $\rho = \frac{a_1}{a_2}$, we obtain

$$B_{2\ell} = \frac{a_1^{\ell+2}(\varepsilon_1 - \varepsilon_2)E_0\delta_{1\ell} - \ell\rho^{2\ell+1}(\varepsilon_1 - \varepsilon_2)B_{3\ell}}{\ell\varepsilon_1 - \ell\rho^{2\ell+1}(\varepsilon_1 - \varepsilon_2) + (\ell+1)\varepsilon_2} \quad (3.65)$$

$$B_{3\ell} = a_2^{\ell+2} \frac{(\varepsilon_2 - \varepsilon_3)[\ell\varepsilon_1 + (\ell+1)\varepsilon_2] + \rho^{2\ell+1}(\varepsilon_1 - \varepsilon_2)[\ell\varepsilon_3 + (\ell+1)\varepsilon_2]}{[\ell\varepsilon_2 + (\ell+1)\varepsilon_3][\ell\varepsilon_1 - (\ell+1)\varepsilon_2] + \ell(\ell+1)\rho^{2\ell+1}(\varepsilon_1 - \varepsilon_2)(\varepsilon_3 - \varepsilon_2)} E_0\delta_{1\ell} \quad (3.66)$$

Notice that the Kronecker delta $\delta_{\ell 1}$ is equal to 0 when $\ell \neq 1$ therefore

$$A_{11} = \frac{B_{21}}{a_1^3} + A_{21} \quad (3.67)$$

$$A_{21} = \frac{B_{31} - B_{21}}{a_2^3} - E_0 \quad (3.68)$$

$$B_{21} = \frac{a_1^3(\varepsilon_1 - \varepsilon_2)E_0 - \rho^3(\varepsilon_1 - \varepsilon_2)B_{31}}{\varepsilon_1 - \rho^3(\varepsilon_1 - \varepsilon_2) + 2\varepsilon_2} \quad (3.69)$$

$$B_{31} = a_2^3 \frac{(\varepsilon_2 - \varepsilon_3)(\varepsilon_1 + 2\varepsilon_2) + \rho^3(\varepsilon_1 - \varepsilon_2)(\varepsilon_3 + 2\varepsilon_2)}{(\varepsilon_2 + 2\varepsilon_3)(\varepsilon_1 - 2\varepsilon_2) + 2\rho^3(\varepsilon_1 - \varepsilon_2)(\varepsilon_3 - \varepsilon_2)} E_0 \quad (3.70)$$

To find the polarizability α we proceed as in the end of section 3.2, focusing only on the potential of the region 3, so that we obtain:

$$\alpha = 4\pi\varepsilon_3 a_2^3 \frac{(\varepsilon_2 - \varepsilon_3)(\varepsilon_1 + 2\varepsilon_2) + \rho^3(\varepsilon_1 - \varepsilon_2)(\varepsilon_3 + 2\varepsilon_2)}{(\varepsilon_2 + 2\varepsilon_3)(\varepsilon_1 - 2\varepsilon_2) + 2\rho^3(\varepsilon_1 - \varepsilon_2)(\varepsilon_3 - \varepsilon_2)} \quad (3.71)$$

3.3.1 Nano-shells: tuning the resonance frequency

The formula for polarizability calculated in the previous section and presented in equation 3.71 can be used for two different kind of metal nanoparticles: the proper *core-shell* nanoparticles, where a metal core is coated with a dielectric shell, and the *nano-shell* nanoparticles, where a dielectric core is coated with a metal shell.

Mathematically, this corresponds to choosing which one of the permittivities present in equation 3.71 is a complex metal permittivity which is function of the frequency (as the one we calculated in section 2.1 and presented in equation 2.16).

Specifically, when ε_1 is a metal permittivity and ε_2 a real constant dielectric permittivity, equation 3.71 represents a proper *core-shell* nanoparticle, while, when ε_1 a real constant dielectric permittivity and ε_2 is a metal permittivity, equation 3.71 represents a *nano-shell*.

Both configurations comes with vantages and disadvantages depending to the application they are tailored to. While the calculation for the heat production, we will present in the following chapter, can be used in both cases, in our characterization we will focus on *nano-shell* particles, because, their Localized Plasmon Resonance is a function of the radius ratio $\rho = \frac{a_1}{a_2}$. This effect is shown in figure 3.7 where the

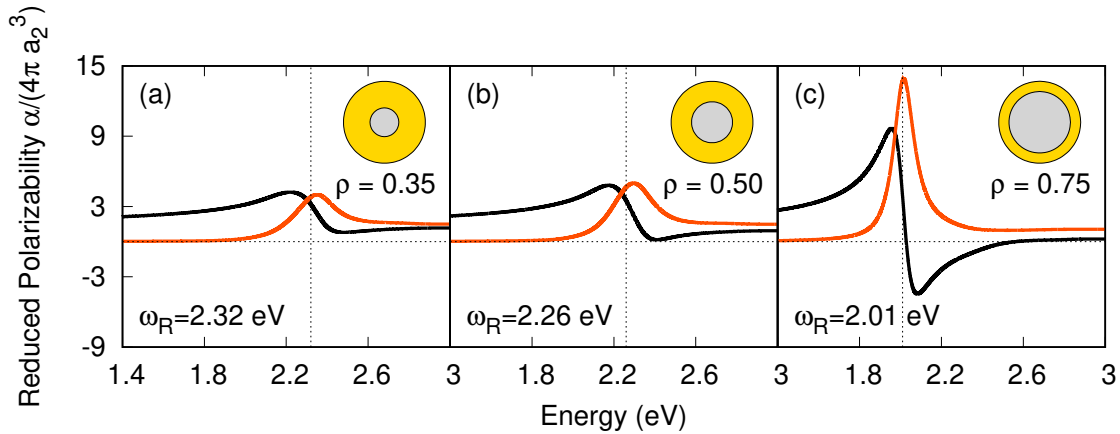


Figure 3.7: Real and Imaginary parts of the Reduced Polarizability for a gold nanoshell with a silica core coated with a gold shell and dissolved in water. The polarizability is presented for different radius ratio: (a) $\rho = 0.35$; (b) $\rho = 0.5$; (c) $\rho = 0.75$;

real and the imaginary parts of the reduced polarizability for gold *nano-shells* with

a silica core and dissolved in water, with different radius ratio. In fig 3.7a we have $\rho = 0.35$ corresponding to a resonance at $\hbar\omega_R = 2.32$ eV, in fig 3.7b we have $\rho = 0.5$ corresponding to a resonance at $\hbar\omega_R = 2.26$ eV, finally in fig 3.7, we have $\rho = 0.75$ corresponding to a resonance at $\hbar\omega_R = 2.01$ eV.

This characteristics is particularly useful for thermal therapy applications, because it allows to choose a configuration resonating in the near infrared, which is the frequency range at which human bodies are more “transparent” to electromagnetic radiation, that is (as mentioned in the introduction) an important factor to optimize the effectiveness of these techniques.

Chapter 4

Heat

We will now enter at the heart of our work: the evaluation of the heat produced in a nano-shell when illuminated by an external source of light.

In general, metal nanoparticles acts as local heat sources when illuminated at any frequency, however when the exciting energy for photon matches the localized surface plasmons resonance the heat generation is amplified by the enhancement of the local fields and currents.

A formula for the heat produced by a spherical nanoparticle is known in the literature [7],

$$Q(\omega) = k\alpha''(\omega)I_0 \quad (4.1)$$

where $k = \frac{\omega}{c}$, $I_0 = \frac{c\varepsilon_0|E_0|^2}{2}$ and c is the speed of light.

However, despite nano-shell particles are a very interesting candidate for thermal therapy and are already under scrutiny [8], a proper formula allowing to calculate the heat produced by illuminating a nano-shell particle is, at the best of our knowledge, missing.

In this chapter we will use the results obtained in for the description of the electric potential in a metal nano-shell to calculate an exact formula for the heat produced in these structures. We will also present a characterization, showing how this calculation gives a better insight on how to realize the perfect design of a nano-shell synthesized for thermal therapy applications.

4.1 Back to the Electromagnetic Problem

By [9], we know that in a linear medium the total electrostatic energy is given by:

$$W = \frac{1}{2} \int_V \mathbf{J} \cdot \mathbf{E} d^3r \quad (4.2)$$

If we consider the nano-shell particle, by the model described in section 3.3 the polarization currents to be found are

$$\mathbf{J} = \omega \varepsilon_0 \varepsilon_m'' \mathbf{E} \quad (4.3)$$

therefore the heat dissipation of our nanoparticle is given by

$$W = \frac{\omega}{2} \varepsilon_0 \varepsilon_m'' \int_{V_m} |\mathbf{E}_m|^2 d^3r \quad (4.4)$$

where V_m is the volume occupied by the metal.

Recalling that the potential in the region enclosed by the metal is given by

$$\Phi_m(r, \theta, \omega) = A_{21}(\omega) r \cos(\theta) + B_{21}(\omega) \frac{\cos(\theta)}{r^2} \quad (4.5)$$

where $A_{21}(\omega)$ and $B_{21}(\omega)$ were defined in equations 3.67-3.70. We can now define:

$$p_3 = \frac{B_{31}}{a_2^3 E_0} \quad (4.6)$$

this way, we have that:

$$B_{21}(\omega) = a_2^3 \frac{\rho^3 (1 - p_3) (\varepsilon_h - \varepsilon_m) E_0}{(\varepsilon_h + 2\varepsilon_m) - \rho^3 (\varepsilon_h - \varepsilon_m)} \quad (4.7)$$

so that we can now define:

$$p_2 = \frac{B_{21}}{a_2^3 E_0} = - \frac{\rho^3 (p_3 - 1) (\varepsilon_h - \varepsilon_m)}{(\varepsilon_h + 2\varepsilon_m) - \rho^3 (\varepsilon_h - \varepsilon_m)} \quad (4.8)$$

which allows us to rewrite A_{21} as:

$$A_{21}(\omega) = (p_3 - p_2 - 1) E_0 \quad (4.9)$$

If now we consider the coefficient $p_3 - 1 - p_2$ and the definition of p_2 given in 4.8,

it's easy to show that:

$$p_3 - 1 - p_2 = (p_3 - 1) \left[1 + \frac{\rho^3(\varepsilon_h - \varepsilon_m)}{(\varepsilon_h + 2\varepsilon_m) - \rho^3(\varepsilon_h - \varepsilon_m)} \right]$$

which simplifies into:

$$p_3 - 1 - p_2 = \frac{(p_3 - 1)(\varepsilon_h + 2\varepsilon_m)}{(\varepsilon_h + 2\varepsilon_m) - \rho^3(\varepsilon_h - \varepsilon_m)}. \quad (4.10)$$

Replacing in 4.5 we get:

$$\begin{aligned} \Phi_m(r, \theta, \omega) = & \frac{(p_3 - 1)(\varepsilon_h + 2\varepsilon_m)}{(\varepsilon_h + 2\varepsilon_m) - \rho^3(\varepsilon_h - \varepsilon_m)} E_0 r \cos(\theta) + \\ & - a_2^3 \frac{\rho^3(p_3 - 1)(\varepsilon_h - \varepsilon_m)}{(\varepsilon_h + 2\varepsilon_m) - \rho^3(\varepsilon_h - \varepsilon_m)} E_0 \frac{\cos(\theta)}{r^2} \end{aligned} \quad (4.11)$$

This last we can recast as:

$$\Phi_m(r, \theta, \omega) = \frac{(p_3 - 1)E_0}{(\varepsilon_h + 2\varepsilon_m) - \rho^3(\varepsilon_h - \varepsilon_m)} \left[(\varepsilon_h + 2\varepsilon_m)r \cos(\theta) - a_2^3 \rho^3(\varepsilon_h - \varepsilon_m) \frac{\cos(\theta)}{r^2} \right] \quad (4.12)$$

Let

$$\zeta(\omega) = \frac{(p_3 - 1)}{(\varepsilon_h + 2\varepsilon_m) - \rho^3(\varepsilon_h - \varepsilon_m)} \quad (4.13)$$

therefore

$$\Phi_m(r, \theta, \omega) = \zeta(\omega) E_0 \left[(\varepsilon_h + 2\varepsilon_m)r \cos(\theta) - a_2^3 \rho^3(\varepsilon_h - \varepsilon_m) \frac{\cos(\theta)}{r^2} \right]. \quad (4.14)$$

Now we proceed to find the radial and the angular components of the electric field

$$E_m^r = - \frac{\partial \Phi_m}{\partial r} = -\zeta(\omega) \cos(\theta) E_0 \left[(\varepsilon_h + 2\varepsilon_m) - 2a_2^3 \rho^3(\varepsilon_h - \varepsilon_m) \frac{1}{r^3} \right] \quad (4.15)$$

$$E_m^\theta = - \frac{1}{r} \frac{\partial \Phi_m}{\partial \theta} = \zeta(\omega) \sin(\theta) E_0 \left[(\varepsilon_h + 2\varepsilon_m) - a_2^3 \rho^3(\varepsilon_h - \varepsilon_m) \frac{1}{r^3} \right] \quad (4.16)$$

Therefore

$$|E_m^r|^2 = |\zeta(\omega)|^2 |\omega| \cos^2(\theta) |E_0|^2 \left(|\varepsilon_h + 2\varepsilon_m|^2 + 4a_2^6 \rho^6 |\varepsilon_h - \varepsilon_m|^2 \frac{1}{r^6} - 2a_2^3 \rho^3 [(\varepsilon_h + 2\varepsilon_m)(\varepsilon_h - \varepsilon_m)^* + (\varepsilon_h - \varepsilon_m)(\varepsilon_h + 2\varepsilon_m)^*] \frac{1}{r^3} \right) \quad (4.17)$$

and

$$|E_m^\theta|^2 = |\zeta(\omega)|^2 \sin^2(\theta) |E_0|^2 \left(|\varepsilon_h + 2\varepsilon_m|^2 + a_2^6 \rho^6 |\varepsilon_h - \varepsilon_m|^2 \frac{1}{r^6} - a_2^3 \rho^3 [(\varepsilon_h + 2\varepsilon_m)(\varepsilon_h - \varepsilon_m)^* + (\varepsilon_h - \varepsilon_m)(\varepsilon_h + \varepsilon_m)^*] \frac{1}{r^3} \right). \quad (4.18)$$

We notice that

$$(\varepsilon_h + 2\varepsilon_m)(\varepsilon_h - \varepsilon_m^*) + (\varepsilon_h - \varepsilon_m)(\varepsilon_h + 2\varepsilon_m^*) = 2(\varepsilon_h^2 - 2|\varepsilon_m|^2 + \varepsilon_h \varepsilon_m'), \quad (4.19)$$

knowing that $|E_m|^2 = |E_m^r|^2 + |E_m^\theta|^2$ we can write:

$$|E_m|^2 = |\zeta(\omega)|^2 |E_0|^2 \left(|\varepsilon_h + 2\varepsilon_m|^2 + a_2^6 \rho^6 |\varepsilon_h - \varepsilon_m|^2 [1 + 3 \cos^2(\theta)] \frac{1}{r^6} - 2a_2^3 \rho^3 \left[\varepsilon_h^2 - 2|\varepsilon_m|^2 + \varepsilon_h \varepsilon_m' \right] \frac{1}{r^3} \right). \quad (4.20)$$

Thus we have to solve

$$W = \omega \pi \varepsilon_0 \varepsilon''_m |\zeta(\omega)|^2 |E_0|^2 \left(|\varepsilon_h + 2\varepsilon_m|^2 \int_0^\pi \int_{a_1}^{a_2} r^2 \sin(\theta) dr d\theta + a_2^6 \rho^6 |\varepsilon_h - \varepsilon_m|^2 \int_0^\pi \int_{a_1}^{a_2} \frac{1}{r^4} [1 + 3 \cos(\theta)] \sin(\theta) dr d\theta - 2a_2^3 \rho^3 \left(\varepsilon_h^2 - 2|\varepsilon_m|^2 + \varepsilon_h \varepsilon_m' \right) \int_0^\pi \int_{a_1}^{a_2} \frac{1}{r} [1 + \cos^2(\theta)] \sin(\theta) dr d\theta \right) \quad (4.21)$$

which leads to:

$$W(\omega) = \frac{2}{3}a_2^3\pi\varepsilon_0\omega\varepsilon''_m(\omega)|\zeta(\omega)|^2 \left[(1 - \rho^3) \left(|\varepsilon_h + 2\varepsilon_m|^2 + 2\rho^3|\varepsilon_h + \varepsilon_m|^2 \right) - 8\rho^3 \ln \left(\frac{1}{\rho} \right) \left(\varepsilon_h^2 - 2|\varepsilon_m|^2 + \varepsilon_h\varepsilon'_m \right) \right] |E_0|^2. \quad (4.22)$$

If we now define:

$$\Theta(\omega) = (1 - \rho^3) \left(|\varepsilon_h + 2\varepsilon_m|^2 + 2\rho^3|\varepsilon_h + \varepsilon_m|^2 \right) - 8\rho^3 \ln \left(\frac{1}{\rho} \right) \left(\varepsilon_h^2 - 2|\varepsilon_m|^2 + \varepsilon_h\varepsilon'_m \right); \quad (4.23)$$

we can compact expression 4.22 into:

$$W(\omega) = \frac{2}{3}a_2^3\pi\varepsilon_0\omega\varepsilon''_m(\omega)|\zeta(\omega)|^2\Theta(\omega)|E_0|^2. \quad (4.24)$$

If we now use that the Intensity of the exciting electromagnetic field is:

$$I_0 = \frac{c\varepsilon_0}{2}|E_0|^2$$

equation 4.24 recast into

$$W(\omega) = \frac{4}{3}\pi a_2^3 \frac{\omega\varepsilon''_m(\omega)}{c} I_0 |\zeta(\omega)|^2 \Theta(\omega), \quad (4.25)$$

where one can recognize the volume of the nanoparticle:

$$V = \frac{4}{3}\pi a_2^3$$

So that we can finally recast our formula into:

$$W(\omega) = \frac{VI_0}{c} \omega\varepsilon''_m(\omega)|\zeta(\omega)|^2\Theta(\omega). \quad (4.26)$$

This is a heat dissipation for unit of time. If we now define a typical time:

$$\tau_0 = \frac{1}{\omega_{pl}},$$

where ω_{pl} is the metal plasma frequency as defined in section 2.1. So that, the energy

absorbed from the nano-shell every τ_0 will be:

$$\frac{W(\omega)}{\tau_0} = \frac{VI_0}{c} \frac{\omega}{\omega_{pl}} \varepsilon''_m(\omega) |\zeta(\omega)|^2 \Theta(\omega). \quad (4.27)$$

Allowing us to define a dimensionless quantity:

$$\Omega(\omega) = \frac{\omega}{\omega_{pl}} \varepsilon''_m(\omega) |\zeta(\omega)|^2 \Theta(\omega). \quad (4.28)$$

Including all of the dependency over frequency of the dissipated heat. We will use this last quantity in all of our characterization.

4.2 Results

In figure 4.1(a), we show the dependency over frequency $\Omega(\omega)$ (as defined in the previous section) for a gold nano-shell with silica core and a radius ratio $\rho = 0.5$; In figure 4.1(a) we report the real and the imaginary part of the Reduced polarizability for the same nanoparticle. As one can see in figure 4.1, most of the heat is

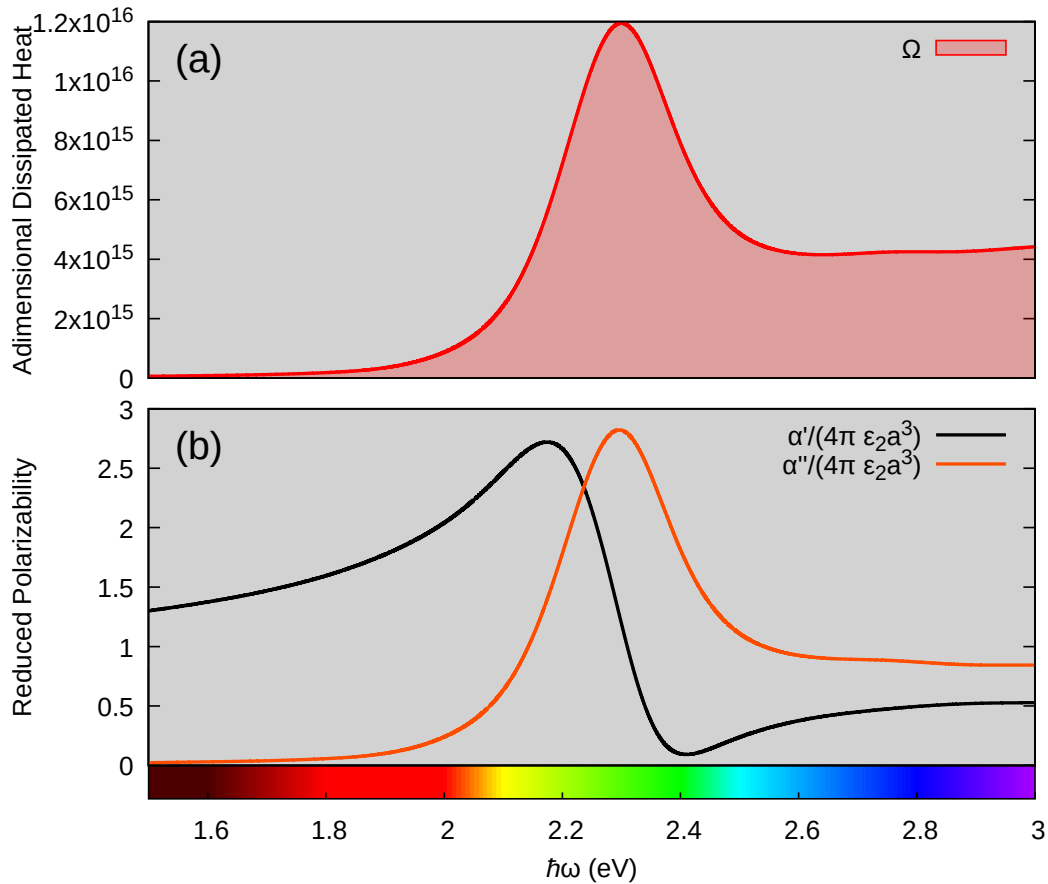


Figure 4.1: (a) Adimensional Dissipated Heat for a gold nano-shell with a silica core and $\rho = 0.5$; (b) Real and imaginary part of the Reduced Polarizability for the same nanoparticle.

dissipated by the nanoparticle around its LSPR which is $\hbar\omega \sim 2.25$ eV and falls in the green region of the visible spectrum. As in the simpler case of a metal sphere, the heat dissipation looks strongly correlated with the imaginary part of the particle polarizability.

It might be worth noting that the Adimensional Dissipated Heat is apparently gigantic, showing an order of magnitude of around 10^{16} . This very high value might be misleading if one does not take into account that, in order to be converted into actual heat it has to be multiplied by the nanoparticle volume V which is very small, and divided by the speed of light in vacuum c which is very big.

In figure 4.2 we present the Adimensional Dissipated Heat Ω as a function of the radius ratio ρ and the energy for photon $\hbar\omega$. Here one can clearly see that, in order

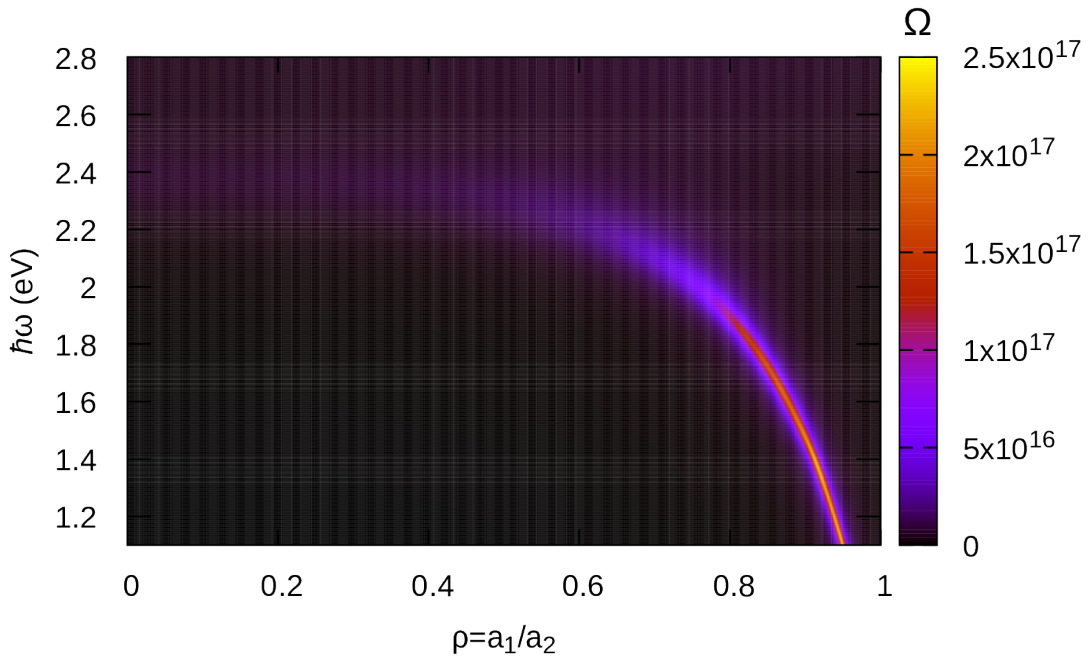


Figure 4.2: Adimensional Dissipated Heat Ω as a function of the radius ratio ρ and the energy for photon $\hbar\omega$.

to synthesize nano-shell particles, resonating in the near infrared (i. e. $\hbar\omega < 1.8$ eV), it is important that the design include a very thin gold shell $\rho > 0.8$.

Although it is known to be more difficult to synthesize thin-shells nanoparticles, so this result might not be saluted with a cheers by the particle-makers, the map presented in figure 4.2 is harbinger of additional and unexpected good news: in the region in which the gold nano-shells resonate in the right corner of the spectrum, the produced heat is an order of magnitude larger than what we find for a thick nano-shell (e. g. for $\rho \sim 0.5$ $\Omega \sim 10^{16}$, while for $\rho > 0.8$ $\Omega \sim 10^{17}$).

Chapter 5

Conclusions

The heat dissipated by a gold nano-shell nanoparticle with silica core, illuminated by an external excitation field, was studied. Using the quasistatic approximation, obtaining the Drude's model with a classical treatment and using an electromagnetic point of view to describe the nanoparticle's potential and electrostatic total energy. We obtained that the nanoparticle has an adimensional heat dissipated in order of magnitude of around 10^{16} and a resonance near the infrared part of the spectrum. This result is useful for photothermal cancer therapy since gold is bio-compatible element with low toxicity and its plasmonic frequency is in the infrared that is the NIR biological transparency window also it can be applied to hyperthermia for cancer therapy to treat skin and breast cancer. Even though we have to consider that a nano-shell nanoparticle that suits this features is very thin, and it makes it difficult to be fabricated. Furthermore, is important to mention that the heat produced by a thick nanoparticle is larger the obtained from the thin ones.

Bibliography

- [1] Baburin, A., Merzlikin, A., Baryshev, A., Ryzhikov, I., Panfilov, Y., and Rodionov, I. (2019). *Silver-based plasmonics: golden material platform and application challenges*. *Optical Materials Express*, 9, 611.
- [2] Baffou, G., Cichos, F., and Quidant, R. (2020). *Applications and Challenges of Thermoplasmonics*. *Nature Materials*.
- [3] Bayda, S., Adeel, M., Tuccinardi, T., Cordani, M., and Rizzolio, F. (2019). *The History of Nanoscience and Nanotechnology: From Chemical–Physical Applications to Nanomedicine*. *Molecules*, 25(1), 112.
- [4] Bohren, C. F., Huffman, D. R. (2008). *Absorption and Scattering of Light by Small Particles*. John Wiley and Sons.
- [5] Caicedo, K., Cathey, A., Infusino, M., Aradian, A., and Veltri, A. (2022). *Gain-driven singular resonances in active core-shell and nano-shell plasmonic particles*. *Journal of the Optical Society of America B*, 39, 107-116.
- [6] Cherukuri, P., Glazer, E. S., and Curley, S. A. (2010). *Targeted Hyperthermia Using Metal Nanoparticles*. *Adv. Drug Deliv. Rev.*, 62, 339–345.
- [7] Gillibert, R., Colas, F., de La Chapelle, M. L., and Gucciardi, P. G. (2020). *Heat Dissipation of Metal Nanoparticles in the Dipole Approximation*. Springer
- [8] Hirsch, L. R., Stafford, R. J., Bankson, J. A., Sershen, S. R., Rivera, B., Price, R. E., ... West, J. L. (2003). *Nanoshell-mediated near-infrared thermal therapy of tumors under magnetic resonance guidance*. *Proceedings of the National Academy of Sciences*, 100(23), 13549–13554.
- [9] Jackson, J. D. (1999) *Classical Electrodynamics*. John Wiley and Sons.
- [10] Johnson, P. B., and Christy, R. W. (1972). *Optical Constants of the Noble Metals*. *Physical Review B*, (6), 4370-4379.

- [11] Kuppe, C., Rusimova, K. R., Ohnoutek, L., Slavov, D., Valev, V. K. (2020) *"Hot" in Plasmonics: Temperature-Related Concepts and Applications of Metal Nanostructures* Advance Optical Materials.
- [12] Lal, S., Clare, S. E., and Halas, N. J. (2008). *Nanoshell-Enabled Photothermal Cancer Therapy: Impending Clinical Impact*. Acc. Chem. Res., 41, 1842.
- [13] Lim, Z. Z. J., Li, J. E. J., Ng, C. T., Yung, L. Y. L., and Bay, B. H. (2011). *Gold Nanoparticles in Cancer Therapy*. Acta Pharmacol. Sin., 32, 983–990.
- [14] Mishchenko, M. I., Travis, L. D., and Mackowski, D. W. (1996). *T-matrix computations of light scattering by nonspherical particles: A review*. Journal of Quantitative Spectroscopy and Radiative Transfer, 55(5), 535–575.
- [15] Novotny, L., and Hecht, B. (2006). *Principles of Nano-Optics*. Cambridge University Press.
- [16] Oleson, J. R., and Dewhirst, M. W. (1983). *Hyperthermia: An Overview of Current Progress and Problems*. Current Problems in Cancer, 8(6), 1–62.
- [17] Olver, P. J. (2014) *Introduction to Partial Differential Equations*. Undergraduate Texts in Mathematics.
- [18] Sapareto, S. A., and Dewey, W. C. (1984). *Thermal Dose Determination in Cancer Therapy*. Int. J. Radiation Oncology Biol. Phys., 10, 787–800.
- [19] Veltri, A., and Ashod, A. (2012). *Optical response of a metallic nanoparticle immersed in a medium with optical gain* Physical Review B, 85(11).
- [20] Veltri, A., Chipouline, A., and Aradian, A. (2016). *Multipolar, time-dynamical model for the loss compensation and lasing of a spherical plasmonic nanoparticle spaser immersed in an active gain medium*. Scientific Reports, 6(1).